3D-2D *Known-Component* Registration for Metal Artifact Reduction in Cone-Beam CT

A. Uneri, T. Yi, X. Zhang, J. W. Stayman, P. Helm, G. M. Osgood, N. Theodore, J. H. Siewerdsen

Abstract—Intraoperative cone-beam CT (CBCT) is increasingly used for surgical navigation and validation of surgical device placement. In spine surgery, for example, CBCT provides visualization of spinal pedicle screws relative to target anatomy and adjacent structures. In the surgical settings, however, high attenuation objects in the field of view are often the norm, producing severe streak artifacts that can confound visualization in precisely the area of interest. In this work, a new method for metal artifact reduction (MAR) is introduced that uses prior information of the shape of surgical instruments to reduce or eliminate metal artifacts.

The approach leverages concepts from conventional MAR (often limited by segmentation error [1]) and more advanced *known-component* (KC) reconstruction (KC-Recon) [2], maintaining the speed and simplicity of simple MAR with the power of prior information as in KC-Recon. The proposed "KC-MAR" approach uses 3D-2D registration of the component model to precisely identify the component in the projection domain, thus overcoming conventional pitfalls associated with (3D or 2D) segmentation in conventional MAR. The result (projected region of the registered component) is then inpainted as in conventional MAR using 2D interpolation or more advanced polyenergetic inpainting. Image reconstruction is performed either by 3D filtered back-projection (FBP, the nominal approach in this work) or iterative model-based iterative reconstruction (MBIR) with corresponding benefits to low-dose performance.

The KC-MAR method was investigated in phantom and cadaver studies presenting a range of challenging metal artifact. Algorithm parameters were investigated in phantom experiments using simple (sphere) components ranging in size and composition. The results were translated to a cadaver study involving spinal pedicle screw placement imaged using an interventional O-Arm (Medtronic, Littleton MA). KC-MAR images were assessed in terms of visualization of the screw within cortical margins adjacent to the spinal cord, showing strong reduction in metal artifacts without sensitivity to conventional segmentation errors, maintaining the speed and simplicity of FBP (but also compatible with MBIR), and providing confident visualization adjacent to instrumentation.

Index Terms—Metal artifact reduction, 3D-2D registration, cone-beam CT imaging

I. Introduction

Metal instrumentation within the field of view (FoV) of CT / CBCT systems can cause severe streak artifacts that degrade image quality and confound confirmation of device placement. Such artifacts are attributable to several effects, including beam-hardening, scatter, and photon starvation [1]. Metallic objects such as prosthetic implants or surgical instruments are routinely introduced in the FoV in image-guided interventions, where they frequently challenge visualization of the device relative to target anatomy and adjacent critical anatomy. In spine surgery, for example, such artifacts arising from pedicle screws can confound visualization of screw placement adjacent to the spinal cord – precisely the region of interest to identify possible breach of the pedicle cortex. Clear visualization right up to the boundary of the screw is required to confidently assure safe delivery of the surgical product.

Metal artifacts originate from data inconsistency and/or photon starvation caused by strong energy-dependent attenuation. A fairly broad range of "metal artifact reduction" (MAR) methods have been proposed to correct or compensate such errors. Algorithms can be considered in two broad categories: i) those that model the physics of beam hardening, noise, etc., implemented within a form of iterative model-based reconstruction; and ii) methods that simply modify the measured projection data within affected regions of strong attenuation (e.g., interpolation / inpainting) [3], [4]. A fundamental problem underlying such approaches involves accurate delineation of the metallic object and strong sensitivity to segmentation error. Segmentation from the initial (uncorrected) 3D image is significantly challenged by the very artifacts the method aims to reduce. Alternatively, segmentation directly in the 2D projection / sinogram domain is challenged by overlapping structures and the need for geometric consistency across the scan orbit.

In image-guided surgery, prior knowledge (e.g. the 3D shape) of components introduced in the FoV is often available, even though the level of information may vary from a simple description (e.g., a deformable, cylindrical tube) to exact, vendor-specific specifications (e.g., CAD drawings for a particular surgical screw). Prior work by Stayman et al. [2] integrated the registration of such known components (KC) within a model-based iterative reconstruction algorithm ("KC-Recon") in a powerful joint registration and reconstruction approach that demonstrated major improvement in image quality compared to FBP (with or without conventional MAR). The KC-Recon approach, however, carries a fairly large computational burden and can challenge time constraints of intraoperative workflow.

In this work, a known-component metal artifact reduction algorithm ("KC-MAR") method is presented that overcomes the sensitivity to segmentation error and preserves the simplicity of conventional MAR (i.e., is compatible with 3D FBP). Recent analogous work by Ruth et al. [5] used the CAD model of knee implants to improve upon an initial, error-prone 3D segmentation, thus leading to improved artifact reduction. Prior information of component shapes (e.g., CAD models specific to a particular device) are used to carry out 3D-2D registration and produce extremely precise and accurate localization of the metallic objects directly in the measurement domain, thus avoiding the potential pitfalls of methods that rely on segmentation.

II. Known-Component Metal Artifact Reduction

An overview of the KC-MAR algorithm is in Figure 1, highlighting the consecutive stages for 3D-2D registration, inpainting of the region in projection of the registered component (by simple interpolation or more sophisticated replacement methods), and 3D image reconstruction (by 3D FBP or other MBIR techniques that usually enjoy improved tradeoffs in noise, resolution, and dose).

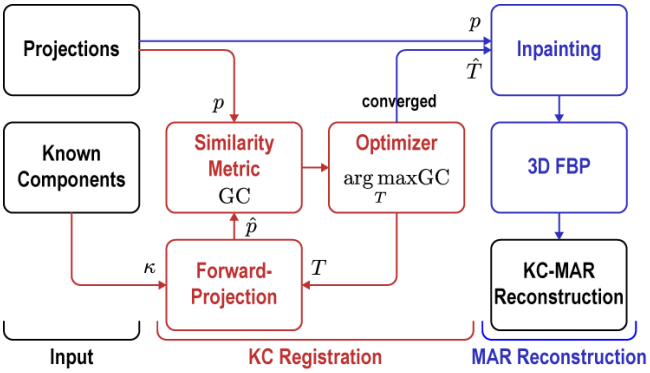

Figure 1. Flowchart for the KC-MAR algorithm depicting the consecutive stages for KC registration and MAR reconstruction with 3D FBP. The registration provides exact localization of the metal components, which are then used to correct (inpaint) projections prior to reconstruction.

A. KC Registration

The details of the 3D-2D registration process for known components ("KC-Reg") have been previously reported by Uneri et al. [6]. A few simplifications to the original approach are possible for KC-MAR, namely: (i) a prior 3D patient image is not necessary, since the components are directly registered to the projections acquired for reconstruction; and (ii) while the KC-Reg method typically operates on just 2–3 projection views, the 3D-2D registration can be rendered extremely precise by using more views – e.g., *all* of the projection views acquired for the 3D reconstruction. To keep runtimes within <1 min in the current work, 6 views with 30° of separation were used, with future work to include a more fully parallelized implementation that suffers little or no additional time penalty in registering more (or all) views.

3D-2D registration of the device components is iterative, beginning with a digitally reconstructed radiograph (DRR) from the input component mesh model:

$$\hat{p}(\kappa, T) = \int_{\vec{r}} \kappa(T)\, \mathrm{d}\vec{r} \tag{1}$$

where each pixel is computed according to the line integral along ray $\vec{r}$ incident on the transformed component κ. The framework was shown to support different component models (e.g., exact technical drawings or simplified parametric models when exact models are not available [6]), and transformation models (e.g. rigid or deformable [7]).

The DRRs are then compared against the actual projections (p) using the gradient correlation (GC) similarity metric [8], defined by the sum of normalized cross-correlation (NCC) of orthogonal image gradients:

$$\begin{aligned} \mathrm{GC}(p, \hat{p}) &= \frac{1}{2}\left\{\mathrm{NCC}(\nabla_x p, \nabla_x \hat{p}) + \mathrm{NCC}\left(\nabla_y p, \nabla_y \hat{p}\right)\right\} \\ \text{s.t. } \mathrm{NCC}(a, b) &= \frac{\sum_i (a_i - \bar{a})(b_i - \bar{b})}{\sqrt{\sum_i (a_i - \bar{a})^2}\sqrt{\sum_i (b_i - \bar{b})^2}} \end{aligned} \tag{2}$$

The GC metric favors the high-intensity gradients from the device component, improving robustness against gradients associated with anatomical structures (e.g., bones).

The objective function for the registration can then be defined as:

$$\hat{T} = \arg\max_T \sum_\theta \mathrm{GC}(p_\theta, \hat{p}_\theta(\kappa, T)) \tag{3}$$

which can be iteratively solved to obtain the component transform ($\hat{T}$) yielding the greatest similarity to the measurements. A stochastic, derivative-free optimization method referred to as the covariance matrix adaptation evolution strategy (CMA-ES) was used, chosen due to its robust convergence and amenability to parallelization [9].

B. MAR Reconstruction

The second stage of KC-MAR uses the registered component to demarcate the region of metal and facilitate sinogram inpainting. Specifically, the DRR of the registered component is computed such that $\hat{p}(\kappa, \hat{T}) > 0$ demarks the metal regions within the original projections, p. Even with an exact component model, the masked region can be dilated to improve robustness against minor errors in registration that can be introduced by manufacturing variation, geometric calibration of the imaging system, or floating precision errors in computing ray-component intersections. The sensitivity of this dilation factor is further analyzed in §III.B.

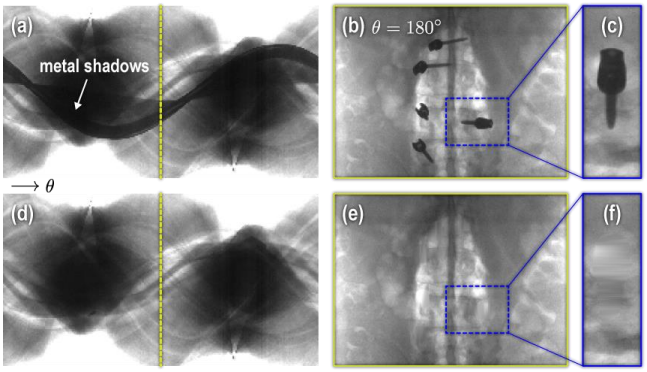

Figure 2. Inpainting of pedicle screws in a cadaver study. (a) The original sinogram with screws, (b) a sample projection, and (c) close-up of an example screw. KC-MAR inpainted counterparts are in d–f, respectively.

The 3D-2D registration yields the transformation by which the shape of the component is forward-projected to precisely define the region to be inpainted. A variety of inpainting methods have been proposed, and in the current work, a simple linear interpolation was used in order to emphasize the benefits of the registration-based approach in isolation of other potential enhancements. This is achieved by first producing a Delaunay triangulation over the convex hull of the masked regions, followed by a barycentric interpolation on each triangle. Repeating this for all θ projections, the region of metal shadow is inpainted for all measurements as shown in Figure 2. The images are then

reconstructed on a 512×512×385 voxel grid with 0.415×0.415×0.415 mm^3 spacing using 3D FBP based on the Feldkamp-Davis-Kress (FDK) algorithm [10].

III. Experimental Evaluation

A. O-Arm CBCT Imaging

CBCT images were acquired using a research prototype (not-for-clinical-use) implementation of the Medtronic O-Arm (Medtronic, Littleton MA). Projection data (1536×1536 pixels at 194 μm pitch) were acquired in dual-gain mode with 4×2 pixel binning. Imaging was performed over a 360° orbit using the manufacturer's high-definition (HD) protocols, giving ~720 projections with ~0.5° radial separation. The geometry was calibrated using a BB phantom [11] to give the projective transforms used in forward / back-projection operations of the algorithm.

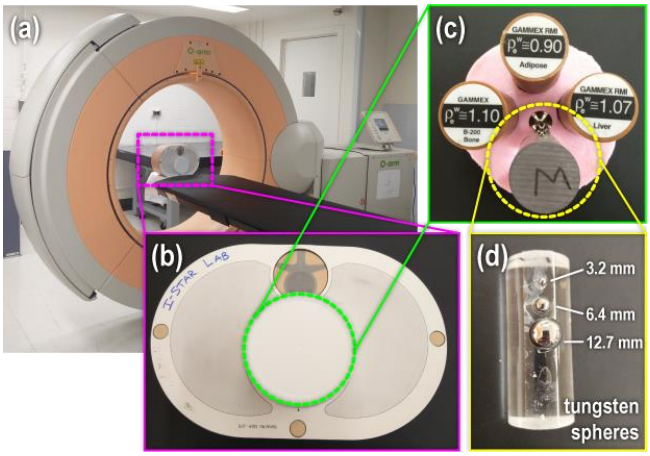

Figure 3. Phantom study. (a) O-Arm setup with (b) abdomen phantom, (c) centerpiece containing tissue-equivalent inserts, and (d) 3 metal spheres of varying diameters attached to an acrylic insert.

B. Phantom Experiments with Simple Components

Phantom studies were performed using chest and phantom models (QRM, Möhrendorf, Germany) shown in Figure 3c including tissue-equivalent inserts (adipose, liver, and bone) and an assortment of metal spheres. The insert assembly was encased in water and placed in the center of the chest or abdomen QRM models. Three spheres of varying diameter (12.7, 6.4, and 3.2 mm) were attached to the acrylic insert (Figure 3d) for three types of metal (tungsten, steel, and titanium). Scans were acquired for each phantom configuration at four dose levels: x-ray tube current of 10, 12, 16, and 25 mA (all at 110 kV).

A simple parametric model of spherical components was employed for KC registration, where each metal sphere was modeled according to 3+1 degrees-of-freedom representing the 3D centroid and diameter. The registration of all 3 spheres was solved simultaneously with collision avoidance enforced by bounding boxes as in [12].

The magnitude of metal artifacts was quantified in terms of a simple "Artifact Magnitude" metric given by the standard deviation (σ) in a homogeneous background region about each metal sphere. Artifact reduction was analyzed as a function of material type (×3), diameter (×3), and dose (×4). The sensitivity to segmentation error as typically evident in conventional MAR was evaluated in a manner that was agnostic / irrespective of a particular segmentation method (and recognizing ongoing work in improving the accuracy of such segmentation): specifically, the boundary of the forward-projected component registration was eroded or dilated over a range ($\Delta\emptyset$) ±3 mm to simulate an arbitrarily small or large segmentation error.

C. Cadaver Study

A second set of experiments was conducted to translate the robustness of algorithm parameters identified in the phantom studies and test the performance of KC-MAR under realistic conditions using a cadaveric human torso (77 year old male, medium body habitus). Pedicle screw placement was performed on the cadaver using a total of 5 pedicle screws in the lumbar spine. Manufacturer-specific CAD models (Solera pedicle screws, Medtronic, Littleton MA) were used as the known components. The component models included a rigid polyaxial screw and its articulating tulip head.

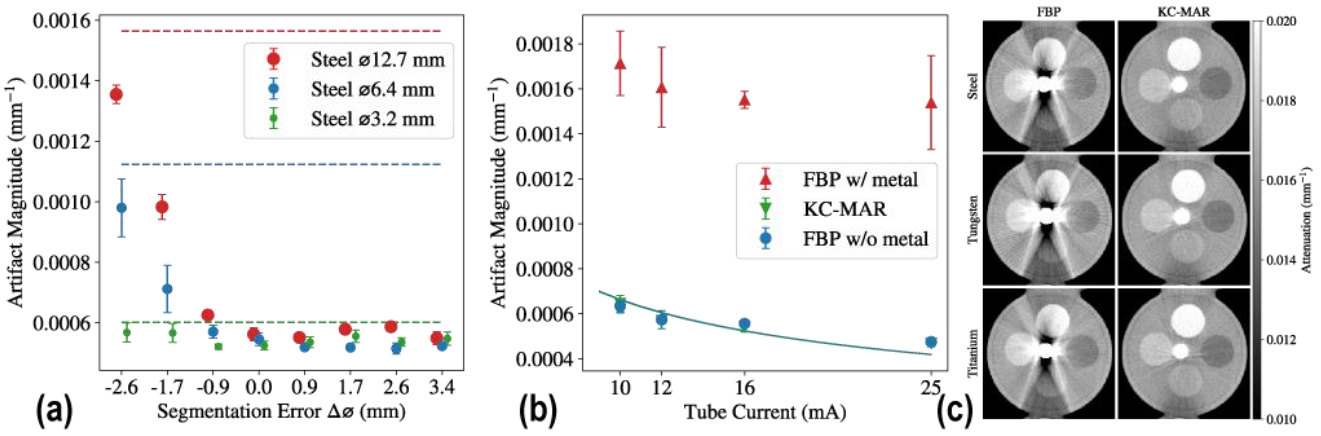

Figure 4. Phantom studies. (a) Evaluation of sensitivity to model mismatch (horizontal lines signify uncorrected values), (b) Artifact magnitude measured as a function of dose with and without metal vs. KC-MAR. (c) Axial image reconstructions with and without KC-MAR for metal spheres of varying material type. The largest of three diameters is shown for each material (and smaller spheres demonstrated similar or better levels of artifact reduction).

IV. Results

A. Phantom Experiments

The performance of KC-MAR in the phantom studies are shown in Figure 4, showing the magnitude of metal artifact as a function of material type, component size (sphere diameter), and dose. Figure 4a shows the sensitivity to segmentation error as often evident in simple MAR – showing the expected result in which underestimation of the true region (simulated here by erosion of the 3D2D-registered region) suffers steep increase in artifact severity, whereas overestimation (dilation) offers a greater degree of stability and robustness to error. KC registration errors were observed to be less than 1 pixel (< 0.5 mm), but a single pixel dilation of the projected component was found to better handle small errors arising from possible variability in device manufacturing or geometric calibration.

Figure 4b shows the performance of KC-MAR as a function of dose, showing the method to be robust even under low dose 3D imaging protocols, whereas methods relying on segmentation in the 3D image would presumably suffer increased segmentation error.

Finally, Figure 4c shows axial images of the phantom insert (adipose, liver, bone, and water in proximity to Ti, W, and Fe spheres). In each case, the largest diameter (12.7 mm) sphere is shown, and similar (or better) results were observed for smaller components. In each case, the KC-MAR approach yielded strong reduction in artifact reduction and improved visualization of adjacent structures.

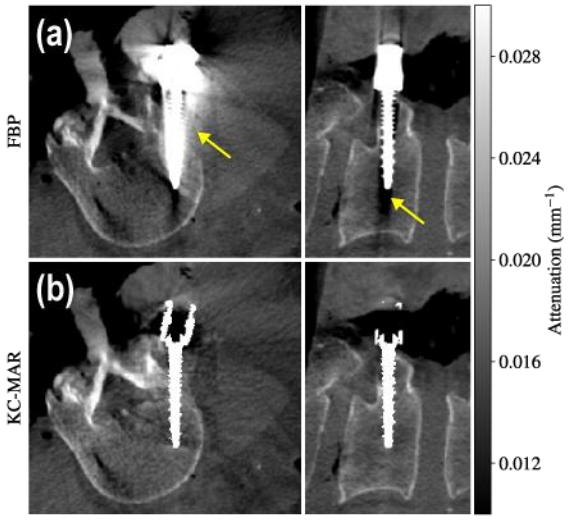

Figure 5. Cadaver study: pedicle screw placement in the L4 vertebra, showing FBP reconstruction (a) without metal artifact reduction and (b) with KC-MAR. The corrected image shows significant reduction in artifacts and allows more reliable visualization of the instrument and adjacent anatomy such as the pedicle cortex and spinal cord.

B. Cadaver Study

The cadaver study investigated KC-MAR performance in real anatomy using a complex component model. Figure 5a shows images of a pedicle screw delivered to the L4 vertebra, where artifacts are seen to confound visualization of adjacent cortical bone. Specifically, the uncorrected image is one in which a surgeon would be challenged to identify whether the screw was delivered with a lateral breach of the pedicle. The KC-MAR image exhibits clear improvement in image quality by reduction of metal artifacts, enabling visualization right up to the edge of the screw – in this case, demonstrating that the lateral pedicle cortex is intact.

V. Discussion

An algorithm for metal artifact reduction was presented based on 3D-2D registration of "known components," offering a variety of potential advantages over existing techniques. The KC-MAR approach maintains the simplicity of conventional MAR (e.g., consistent with 3D FBP and other artifact corrections that may be incorporated in the reconstruction process) but yields a near-perfect localization of the metal object – i.e., does not suffer segmentation errors that are often a limiting factor in conventional MAR. It leverages the power of prior information (i.e., the component model) in a manner similar to KC-Recon [2] but is not bound to joint model-based registration / reconstruction approaches that often carry large computation time that can challenge surgical workflow. In its current implementation (a single GPU GTX TITAN Black [Nvidia, SantaClara CA]), KC-MAR registration required < 1 min with FBP reconstruction in < 2 min. The method benefits from precise models of the metal device but can be extended to simplified parametric models as in [6], with dilation of the resulting region shown to provide robustness to error.

References

[1] M. L. Kataoka, M. G. Hochman, E. K. Rodriguez, P.-J. P. Lin, S. Kubo, and V. D. Raptopolous, "A review of factors that affect artifact from metallic hardware on multi-row detector computed tomography.," *Curr. Probl. Diagn. Radiol.*, vol. 39, no. 4, pp. 125–36.

[2] J. W. Stayman, Y. Otake, J. L. Prince, A. J. Khanna, and J. H. Siewerdsen, "Model-based tomographic reconstruction of objects containing known components.," IEEE *Trans. Med. Imaging*, vol. 31, no. 10, pp. 1837–48, Oct. 2012.

[3] M. Bal and L. Spies, "Metal artifact reduction in CT using tissue-class modeling and adaptive prefiltering.," *Med. Phys.*, vol. 33, no. 8, pp. 2852–9, Aug. 2006.

[4] J. Wei, L. Chen, G. A. Sandison, Y. Liang, and L. X. Xu, "X-ray CT high-density artefact suppression in the presence of bones.," *Phys. Med. Biol.*, vol. 49, no. 24, pp. 5407–18, Dec. 2004.

[5] V. Ruth, D. Kolditz, C. Steiding, and W. A. Kalender, "Metal artifact reduction in X-ray computed tomography using computer-aided design data of implants as prior information," *Invest. Radiol.*, vol. 52, no. 6, pp. 349–359, 2017.

[6] A. Uneri, T. De Silva, J. W. Stayman, G. Kleinszig, S. Vogt, A. J. Khanna, Z. L. Gokaslan, J.-P. Wolinsky, and J. H. Siewerdsen, "Known-component 3D–2D registration for quality assurance of spine surgery pedicle screw placement," *Phys. Med. Biol.*, vol. 60, no. 20, pp. 8007–24, Oct. 2015.

[7] A. Uneri, J. Goerres, T. De Silva, M. W. Jacobson, M. D. Ketcha, S. Reaungamornrat, G. Kleinszig, S. Vogt, A. J. Khanna, J.-P. Wolinsky, and J. H. Siewerdsen, "Deformable 3D-2D registration of known components for image guidance in spine surgery," *Med. Image Comput. Comput. Assist. Interv.*, vol. 19, no. 3, pp. 124–32, 2016.

[8] G. P. Penney, J. Weese, J. A. Little, P. Desmedt, D. L. Hill, and D. J. Hawkes, "A comparison of similarity measures for use in 2-D-3-D medical image registration.," *IEEE Trans. Med. Imaging*, vol. 17, no. 4, pp. 586–95, Aug. 1998.

[9] N. Hansen and A. Ostermeier, "Completely derandomized self-adaptation in evolution strategies.," *Evol. Comput.*, vol. 9, no. 2, pp. 159–95, Jan. 2001.

[10] L. A. Feldkamp, L. C. Davis, and J. W. Kress, "Practical cone-beam algorithm," *J. Opt. Soc. Am. A*, vol. 1, no. 6, pp. 612–9, Jun. 1984.

[11] Y. Cho, D. J. Moseley, J. H. Siewerdsen, and D. a. Jaffray, "Accurate technique for complete geometric calibration of cone-beam computed tomography systems," *Med. Phys.*, vol. 32, no. 4, p. 968, Apr. 2005.

[12] A. Uneri, T. De Silva, J. Goerres, M. Jacobson, M. Ketcha, S. Reaungamornrat, G. Kleinszig, S. Vogt, A. Khanna, G. Osgood, J.-P. Wolinsky, and J. Siewerdsen, "Intraoperative evaluation of device placement in spine surgery using known-component 3D-2D image registration," *Phys. Med. Biol.*, Feb. 2017.